Diabetologia (2023) 66:223–240
https://doi.org/10.1007/s00125-022-05810-6

ARTICLE

Hedgehog interacting protein activates sodium–glucose cotransporter 2 expression and promotes renal tubular epithelial cell senescence in a mouse model of type 1 diabetes

Xin-Ping Zhao[1] · Shiao-Ying Chang[1] · Yuchao Pang[1] · Min-Chun Liao[1] · Junzheng Peng[1] · Julie R. Ingelfinger[2] · John S. D. Chan[1] · Shao-Ling Zhang[1]

Received: 14 April 2022 / Accepted: 17 August 2022 / Published online: 19 October 2022

Abstract

Aims/hypothesis Senescent renal tubular cells may be linked to diabetic kidney disease (DKD)-related tubulopathy. We studied mice with or without diabetes in which hedgehog interacting protein (HHIP) was present or specifically knocked out in renal tubules (*Hhip*^{RT}-KO), hypothesising that local deficiency of HHIP in the renal tubules would attenuate tubular cell senescence, thereby preventing DKD tubulopathy.

Methods Low-dose streptozotocin was employed to induce diabetes in both *Hhip*^{RT}-KO and control (*Hhip*$^{fl/fl}$) mice. Transgenic mice overexpressing *Hhip* in renal proximal tubular cells (RPTC) (*Hhip*^{RPTC}-Tg) were used for validation, and primary RPTCs and human RPTCs (HK2) were used for in vitro studies. Kidney morphology/function, tubular senescence and the relevant molecular measurements were assessed.

Results Compared with *Hhip*$^{fl/fl}$ mice with diabetes, *Hhip*^{RT}-KO mice with diabetes displayed lower blood glucose levels, normalised GFR, ameliorated urinary albumin/creatinine ratio and less severe DKD, including tubulopathy. Sodium–glucose cotransporter 2 (SGLT2) expression was attenuated in RPTCs of *Hhip*^{RT}-KO mice with diabetes compared with *Hhip*$^{fl/fl}$ mice with diabetes. In parallel, an increased tubular senescence-associated secretory phenotype involving release of inflammatory cytokines (IL-1β, IL-6 and monocyte chemoattractant protein-1) and activation of senescence markers (p16, p21, p53) in *Hhip*$^{fl/fl}$ mice with diabetes was attenuated in *Hhip*^{RT}-KO mice with diabetes. In contrast, *Hhip*^{RPTC}-Tg mice had increased tubular senescence, which was inhibited by canagliflozin in primary RPTCs. In HK2 cells, HHIP overexpression or recombinant HHIP increased SGLT2 protein expression and promoted cellular senescence by targeting both ataxia-telangiectasia mutated and ataxia-telangiectasia and Rad3-related-mediated cell arrest.

Conclusions/interpretation Tubular HHIP deficiency prevented DKD-related tubulopathy, possibly via the inhibition of SGLT2 expression and cellular senescence.

Keywords Diabetic nephropathy · Hedgehog interacting protein · Renal tubular cell senescence · Sodium–glucose cotransporter 2

Abbreviations

ATM	Ataxia-telangiectasia mutated
ATR	ATM- and Rad3-related
CDK	Cyclin-dependent kinase
Col 4	Collagen IV
CRCHUM	Centre de recherche du centre hospitalier de l'Université de Montréal
DKD	Diabetic kidney disease
EMT	Epithelial-to-mesenchymal transition
HHIP	Hedgehog interacting protein
Hhip^{RPTC}-Tg	Tg mice overexpressing HHIP in RPTCs
Hhip^{RT}-KO	Renal tubule-specific *Hhip* knockout
IF	Immunofluorescence
IHC	Immunohistochemistry
LDSTZ	Low-dose STZ

✉ Shao-Ling Zhang
shao.ling.zhang@umontreal.ca

[1] Centre de recherche du Centre hospitalier de l'Université de Montréal (CRCHUM), Department of Medicine, Université de Montréal, Montréal, QC, Canada

[2] Harvard Medical School, Pediatric Nephrology Unit, Massachusetts General Hospital, Boston, MA, USA

Research in context

What is already known about this subject?

- Senescent renal tubular cells may be linked to diabetic kidney disease (DKD)-related tubulopathy
- Elevated renal hedgehog interacting protein (HHIP) expression promotes cellular remodelling that subsequently worsens kidney function in humans with type 2 diabetes and in diabetic murine DKD models
- HHIP might promote senescence-associated secretory phenotype (SASP) by the release of excessive soluble HHIP and a variety of inflammatory cytokines in remodelled kidney cells

What is the key question?

- What is the role of HHIP in the renal tubule and how does this link to SASP and DKD pathology in murine type 1 diabetes models?

What are the new findings?

- Tubular HHIP deficiency prevented DKD-related tubulopathy via the inhibition of sodium–glucose cotransporter 2 (SGLT2) expression and tubular cell senescence
- HHIP overexpression or recombinant HHIP directly increased SGLT2 protein expression and promoted cellular senescence by targeting both ataxia-telangiectasia mutated (ATM) and ATM- and Rad3-related-mediated cell arrest

How might this impact on clinical practice in the foreseeable future?

- Novel therapeutic strategies that target HHIP may provide a means to prevent adverse DKD-mediated renal tubular cell remodelling

LTL	Lotus tetragonolobus lectin
MCP1	Monocyte chemoattractant protein-1
2-NBDG	2-(*n*-[7-Nitrobenz-2-oxa-1, 3-diazol-4-yl] amino)-2-deoxyglucose
OCT	Optimal cutting temperature compound
PAS	Periodic Acid Schiff
rHHIP	Recombinant HHIP
RPT	Renal proximal tubule
RPTC	Renal proximal tubular cell
RT-qPCR	Real-time quantitative PCR
SASP	Senescence-associated secretory phenotype
SGLT1	Sodium–glucose cotransporter 1
SGLT2	Sodium–glucose cotransporter 2
STZ	Streptozotocin
Tg	Transgenic
UACR	Urinary albumin/creatinine ratio
WB	Western blotting

Introduction

Diabetic kidney disease (DKD) is the leading cause of kidney failure in the USA, representing ~44% of all cases of kidney failure [1]. Better understanding of drugs that inhibit the renin–angiotensin system and the sodium–glucose cotransporter 2 (SGLT2) has led to usages that are beneficial for slowing the progression of DKD [2, 3]. However, use of these agents does not prevent ultimate progression of DKD. Thus, identification of new molecules and/or understanding molecular mechanisms that might be useful for the development of targeted therapies for individuals at risk of developing DKD are needed.

Fig. 1 (**a**–**c**) Generation of *Hhip*^{RT}-KO (vs *Hhip*$^{fl/fl}$) mice; genotyping of *Hhip*$^{fl/fl}$ vs heterozygous *Hhip*^{RT}-KO (*Hhip*^{RT}-Het) vs *Hhip*^{RT}-KO mice (**a**), WB analysis in the isolated RPTs (**b**) and HHIP IF staining in the kidneys (**c**) are shown. Scale bar, 50 μm. (**d**–**k**) In an LDSTZ model in mice (10–20 weeks old), body weight progression (**d**), longitudinal SBP (**e**) and blood glucose (determined by an Accu-Chek Performa glucose meter; maximal detectable level, 33.5 mmol/l) (**f**) were monitored, together with the following variables: kidney weight/tibia length ratio (**g**); glucose concentration in urine (**h**) and blood (**i**) (measured by the glucose colorimetric kit); UACR (**j**); and GFR/body weight (**k**). Non-diabetic groups were *Hhip*$^{fl/fl}$-CON and *Hhip*^{RT}-KO-CON mice; diabetic groups were *Hhip*$^{fl/fl}$-STZ and *Hhip*^{RT}-KO-STZ mice. Data are shown as mean ± SEM for the indicated numbers of mice. *$p \leq 0.05$, **$p \leq 0.01$ and ***$p \leq 0.001$ for indicated comparisons; $^{\dagger}p \leq 0.05$, $^{\dagger\dagger}p \leq 0.01$ and $^{\dagger\dagger\dagger}p \leq 0.001$ vs *Hhip*$^{fl/fl}$-CON; $^{\ddagger}p \leq 0.05$, $^{\ddagger\ddagger}p \leq 0.01$ and $^{\ddagger\ddagger\ddagger}p \leq 0.001$ vs *Hhip*^{RT}-KO-CON (one-way ANOVA, followed by Bonferroni's post hoc test). BW, body weight; KW, kidney weight; TL, tibia length; WT, wild type

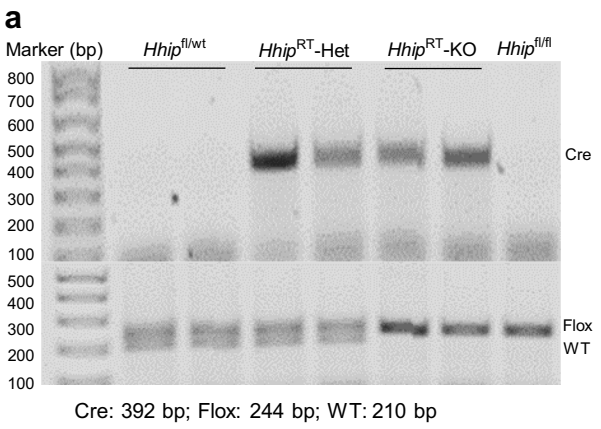
a
Marker (bp)
Hhip fl/wt
Hhip RT-Het
Hhip RT-KO
Hhip fl/fl
800
700
600
500
400
300
200
100
Cre
Flox
WT
Cre: 392 bp; Flox: 244 bp; WT: 210 bp

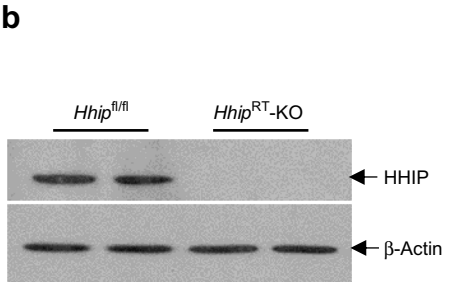
b
Hhip fl/fl
Hhip RT-KO
HHIP
β-Actin

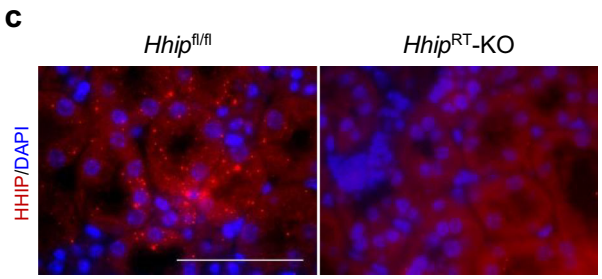
c
Hhip fl/fl
Hhip RT-KO
HHIP/DAPI

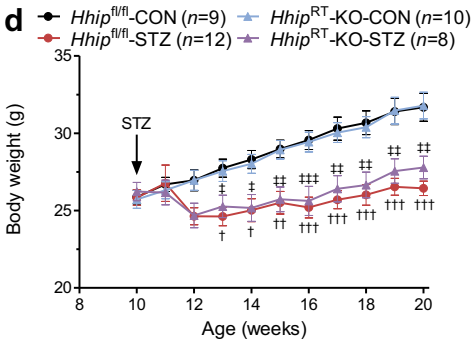
d
Hhip fl/fl-CON (n=9)
Hhip RT-KO-CON (n=10)
Hhip fl/fl-STZ (n=12)
Hhip RT-KO-STZ (n=8)
Body weight (g)
STZ
Age (weeks)

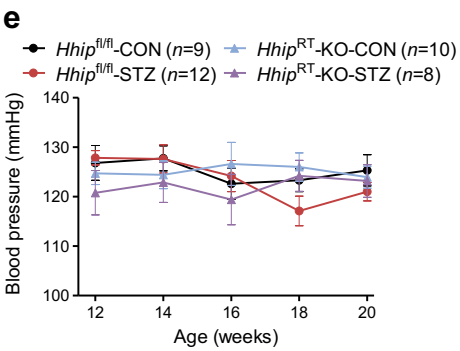
e
Hhip fl/fl-CON (n=9)
Hhip RT-KO-CON (n=10)
Hhip fl/fl-STZ (n=12)
Hhip RT-KO-STZ (n=8)
Blood pressure (mmHg)
Age (weeks)

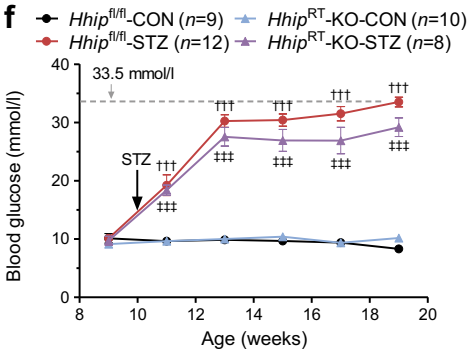
f
Hhip fl/fl-CON (n=9)
Hhip RT-KO-CON (n=10)
Hhip fl/fl-STZ (n=12)
Hhip RT-KO-STZ (n=8)
33.5 mmol/l
STZ
Blood glucose (mmol/l)
Age (weeks)

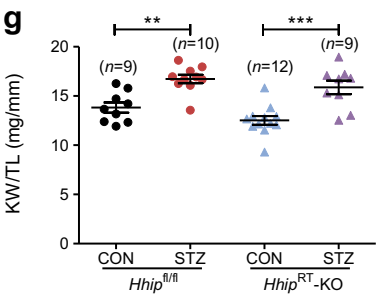
g
KW/TL (mg/mm)
CON
STZ
Hhip fl/fl
Hhip RT-KO

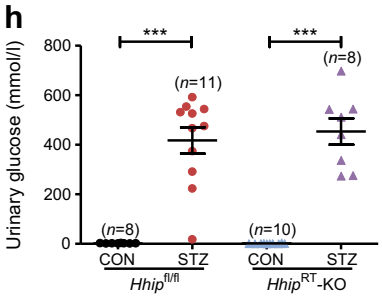
h
Urinary glucose (mmol/l)
CON
STZ
Hhip fl/fl
Hhip RT-KO

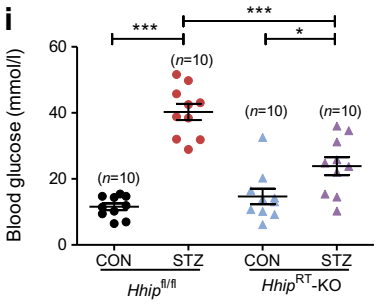
i
Blood glucose (mmol/l)
CON
STZ
Hhip fl/fl
Hhip RT-KO

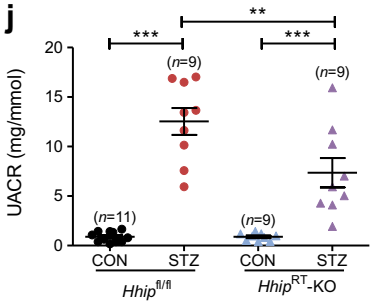
j
UACR (mg/mmol)
CON
STZ
Hhip fl/fl
Hhip RT-KO

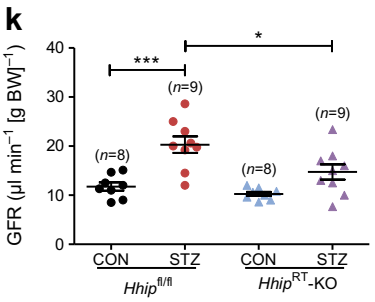
k
GFR (μl min−1 [g BW]−1)
CON
STZ
Hhip fl/fl
Hhip RT-KO

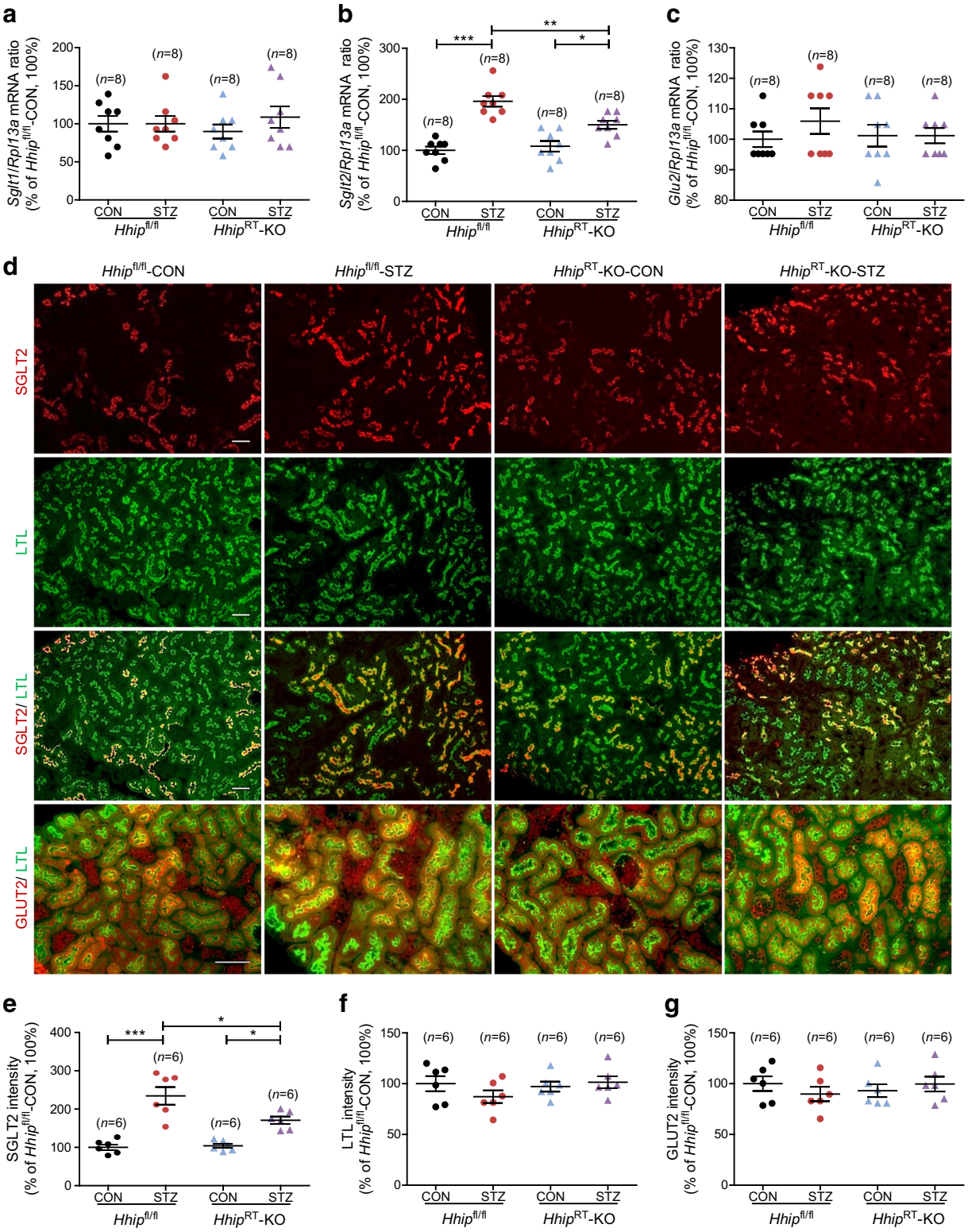

Fig. 2 Glucose transporter gene expression (*Sglt1*, *Sglt2* and *Glut2*) in the kidneys of mice at 20 weeks of age. (**a**–**c**) RT-qPCR in isolated RPTs, showing *Sglt1* (**a**), *Sglt2* (**b**) and *Glut2* mRNA (**c**). mRNA change in each gene was determined and normalised to its own *Rpl13a* mRNA. (**d**–**g**) Representative images of IF staining for SGLT2 (red), LTL (green) and GLUT2 (red) in the kidneys are shown (**d**), together with semi-quantification of IF staining for SGLT2 (**e**), LTL (**f**) and GLUT2 (**g**). Scale bar, 50 μm. Data are shown as mean ± SEM, for the indicated numbers of mice. *$p \leq 0.05$, **$p \leq 0.01$ and ***$p \leq 0.001$ (one-way ANOVA, followed by Bonferroni's post hoc test)

Tubular atrophy and tubulointerstitial fibrosis have been recognised as hallmarks of chronic kidney disease, including DKD [4, 5]. Stressed renal tubular epithelial cells, via an epithelial-to-mesenchymal transition (EMT), are key to the initiation and progression of kidney damage and repair [6]. Instead of fully committing to EMT, such cells demonstrate 'epithelial plasticity' and, potentially, may dedifferentiate [7]. Reparative EMT involves either p53 (a tumour suppressor) and $p21^{Cip1}$ (a cyclin-dependent kinase [CDK] inhibitor) or $p16^{Ink4a}$ (a CDK inhibitor)-mediated cell-cycle arrest that actively produces a senescence-associated secretory phenotype (SASP) [8–10]. In addition, the SASP induces senescence in neighbouring cells (a process known as secondary senescence) through the release of inflammatory cytokines, growth factors and extracellular matrix proteins, and promotion of local and/or systemic pathology associated with loss of kidney function; however, the underlying mechanism(s) are incompletely understood [8–10].

Hedgehog interacting protein (HHIP) encodes a protein of 700 amino acids attached to the cell membrane via a glycosylphosphatidylinositol anchor [11–13]. Both intracellular HHIP and soluble HHIP regulate cellular function via either canonical [11–13] and/or non-canonical hedgehog pathways [14, 15]. HHIP is essential in organ development [12, 16] and aberrant HHIP expression has been linked to several human diseases such as pancreatitis [17], chronic obstructive pulmonary disease [18] and certain tumours [19]. HHIP is detectable in renal endothelial and epithelial cells in the normal, mature kidney, as we reported previously [20, 21]. Of note, renal HHIP expression increases markedly during hyperglycaemia in vivo and in high-glucose milieu in vitro [20, 21]. Elevated HHIP expression promotes cellular remodelling via TGF-β1-mediated EMT, which subsequently worsens kidney function in humans with type 2 diabetes mellitus and in mouse models of diabetes and DKD (Akita and *db/db* mice) [20, 21]. Importantly, we found that urinary HHIP production is elevated in early DKD prior to the development of microalbuminuria. Furthermore, this increased urinary HHIP production is positively associated with eGFR and urinary cytokines (IL-1β, IL-6, IL-8 and TGF-β1) in humans with type 2 diabetes [20]. Taken together, these data suggest that HHIP might promote SASP through the release of excessive soluble HHIP and a variety of inflammatory cytokines in remodelled kidney cells, thereby exacerbating the progression of DKD. However, the molecular basis of how and which renal HHIP-producing cells link to SASP and worsen DKD pathology is poorly understood.

In the present work, focusing on renal tubular cells, we speculated that high-glucose-induced HHIP expression promotes cellular senescence and subsequently worsens DKD-mediated tubulopathy. By employing low-dose streptozotocin (LDSTZ) to induce diabetes in mice that have renal tubule-specific *Hhip* knockout ($Hhip^{RT}$-KO) and in their control littermates ($Hhip^{fl/fl}$), we studied the impact of renal tubule HHIP deficiency on overall kidney function and the progression of DKD, including tubulopathy. We validated tubular SASP phenotype in our transgenic (Tg) mice overexpressing HHIP in renal proximal tubular cells (RPTCs) ($Hhip^{RPTC}$-Tg). In addition, primary RPTCs and human RPTCs (HK2) were used to elucidate the underlying mechanism(s) in vitro.

Methods

Animal models $Hhip^{RT}$-KO mice were generated by cross-breeding $Hhip^{fl/fl}$ mice (Cyagen, USA; https://www.cyagen.com/) (C57/BL6J) with a renal tubule-specific *Cre* deleter mouse line ($Pax8^{Cre}$; B6.129P2 (Cg)-$Pax8^{tm1.1(Cre)Mbu}$/J; The Jackson Laboratory, USA; https://legacystrain.jax.org/strain/028196) [22, 23]. We would note that there is no evidence that $Pax8^{Cre}$ affects HHIP expression in the brain and thyroid gland, similar to findings in our $Pax8^{Cre}$ hnRNP F-KO mice (data not shown) [23]. Both sexes of $Hhip^{RT}$-KO mice are phenotypically indistinguishable from $Hhip^{fl/fl}$ mice as adults.

We used LDSTZ (Sigma-Aldrich Canada, Oakville, ON, Canada) as recommended by the NIH Animal Models of Diabetic Complications Consortium (http://www.diacomp.org/, accessed 14 December 2015), in male mice at 10 weeks of age, administering i.p. injections of streptozotocin (STZ) at a dose of ~45–50 mg per kg body weight daily for five consecutive days. Four subgroups of mice were studied, including non-diabetic control mice ($Hhip^{fl/fl}$-CON and $Hhip^{RT}$-KO-CON) and diabetic mice ($Hhip^{fl/fl}$-STZ and $Hhip^{RT}$-KO-STZ). Blood glucose levels (mmol/l) were measured weekly with an Accu-Chek Performa glucose meter (Roche Diagnostics, Laval, QC, Canada) [21, 23]. Mice with blood glucose levels below 16 mmol/l (measured 72 h following the last STZ injection) were excluded from our analyses.

As with several Tg lines overexpressing genes in RPTCs that we have reported [24, 25], our $Hhip^{RPTC}$-Tg mouse line (C57BL/6J) was generated by overexpressing mouse *Hhip* (Myc-*Hhip* [NM_020259.4, 494-2596bp, 700 aa]-Flag) in the RPTCs driven by the kidney-specific, androgen-regulated protein promoter KAP2.

All mice were euthanised at 20 weeks of age by i.p. injection of 75 mg/kg sodium pentobarbital, and the kidneys were removed immediately and either quickly frozen in optimal cutting temperature compound (OCT) or fixed overnight in

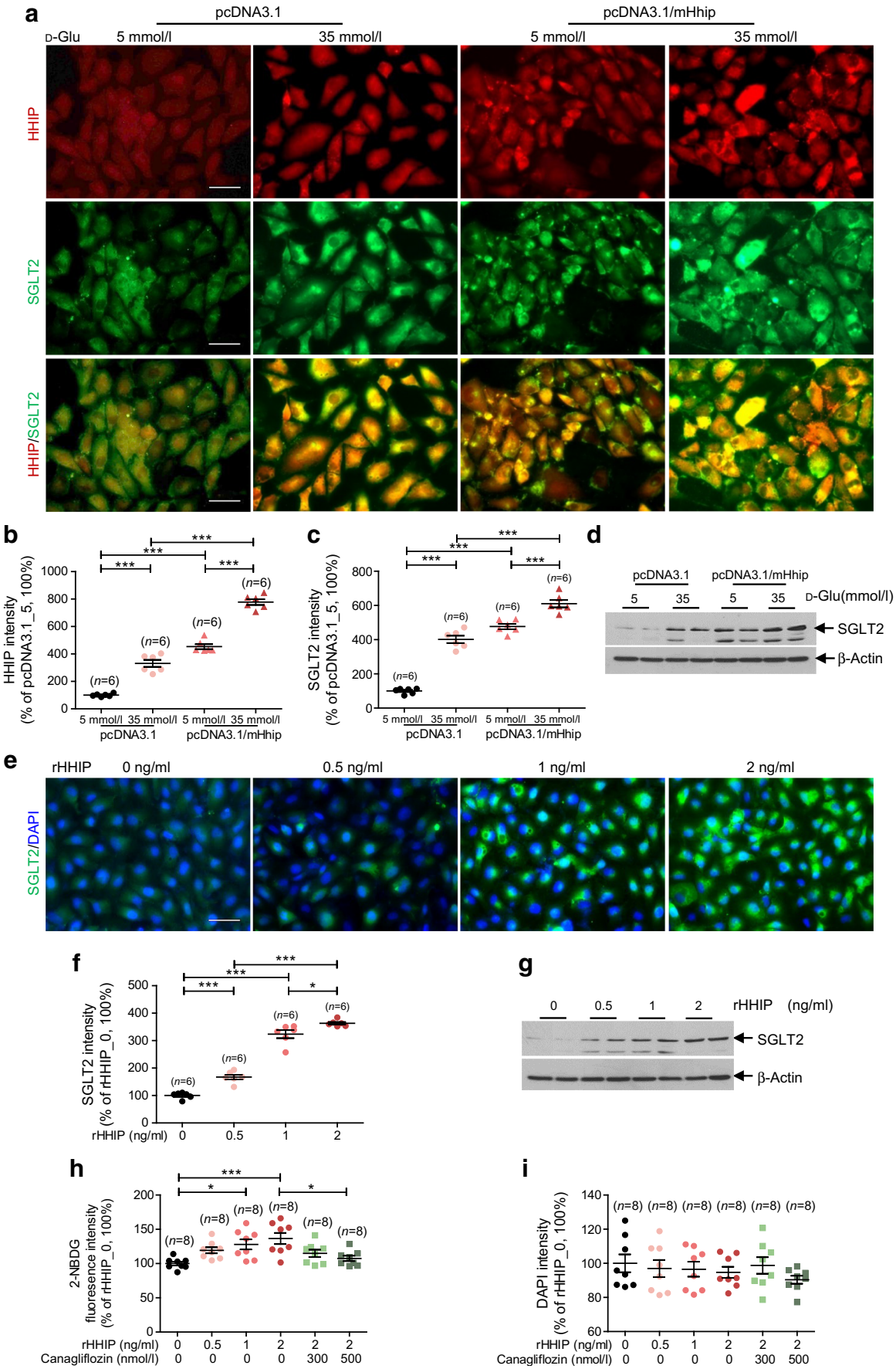
a
pcDNA3.1
pcDNA3.1/mHhip
D-Glu 5 mmol/l 35 mmol/l 5 mmol/l 35 mmol/l
HHIP
SGLT2
HHIP/SGLT2
b
HHIP intensity (% of pcDNA3.1_5, 100%)
5 mmol/l 35 mmol/l 5 mmol/l 35 mmol/l
pcDNA3.1 pcDNA3.1/mHhip
c
SGLT2 intensity (% of pcDNA3.1_5, 100%)
d
pcDNA3.1 pcDNA3.1/mHhip
5 35 5 35 D-Glu(mmol/l)
SGLT2
β-Actin
e
rHHIP 0 ng/ml 0.5 ng/ml 1 ng/ml 2 ng/ml
SGLT2/DAPI
f
SGLT2 intensity (% of rHHIP_0, 100%)
rHHIP (ng/ml) 0 0.5 1 2
g
0 0.5 1 2 rHHIP (ng/ml)
SGLT2
β-Actin
h
2-NBDG fluoresence intensity (% of rHHIP_0, 100%)
rHHIP (ng/ml) 0 0.5 1 2 2 2
Canagliflozin (nmol/l) 0 0 0 0 300 500
i
DAPI intensity (% of rHHIP_0, 100%)
rHHIP (ng/ml) 0 0.5 1 2 2 2
Canagliflozin (nmol/l) 0 0 0 0 300 500

◀ **Fig. 3** The interaction of HHIP and SGLT2 in HK2 cells. (**a**–**d**) Cells overexpressing mouse *Hhip* by transient transfection with the pcDNA3.1/mHhip (vs pcDNA3.1) plasmid (1 μg/μl) were treated with either 5 mmol/l or 35 mmol/l D-glucose for 24 h. Representative images are shown (HHIP, red; SGLT2, green; DAPI, blue) (**a**), together with semi-quantification of IF staining for HHIP (**b**) and SGLT2 (**c**), and WB of SGLT2 expression (**d**). Scale bar, 50 μm. Three separate experiments (duplicated setting per experiment) were performed. (**e**–**g**) Cells were treated with rHHIP dose-dependently for 24 h. Representative images are shown (SGLT2, green; DAPI, blue) (**e**), together with semi-quantification of IF staining for SGLT2 (**f**), and WB of SGLT2 expression (**g**). Scale bar, 50 μm. Three separate experiments (duplicated setting per experiment) were performed. (**h**, **i**) Cellular glucose uptake was measured in HK2 cells treated with rHHIP ± canagliflozin; four separate experiments (duplicated setting per experiment). Data shown as mean ± SEM for the indicated numbers of mice. *$p \leq 0.05$ and ***$p \leq 0.001$ (one-way ANOVA, followed by Bonferroni's post hoc test). D-Glu, D-glucose; pcDNA3.1_5, pcDNA3.1 at 5 mmol/l D-glucose; rHHIP_0, rHHIP 0 ng/ml

4% paraformaldehyde at 4°C before paraffin-embedding [21, 23]. Additional biological samples were processed, collected and stored for analysis.

Animal care and experimental procedures were approved by the Animal Care Committee at the Centre de recherche du centre hospitalier de l'Université de Montréal (CRCHUM). The mice were randomly separated in ventilated cages in specific pathogen free (SPF) conditions under a 12 h light–dark cycle with free access to chow and water at the CRCHUM's animal facility. Both number and suffering of animals were minimised as much as possible.

Physiological studies Body weight (g) was recorded weekly. Systolic BP (SBP, mmHg) was measured longitudinally from 10 to 20 weeks of age following 1 week of pre-training and was monitored by the tail-cuff method with a BP-2000 Blood Pressure Analysis System (Visitech Systems, Apex, NC, USA), as reported elsewhere [21, 23]. Before euthanasia, urine samples were collected from mice individually housed in metabolic cages for 6 h; the GFR (μl min^{-1} [g body weight]$^{-1}$) was measured by the FITC–inulin method as recommended by the Animal Models of Diabetic Complications Consortium (http://www.diacomp.org/, accessed 17 February 2014) [21, 23, 26].

Kidney weight (mg) and tibia length (mm) were recorded after the mice were euthanised. Urinary albumin/creatinine ratio (UACR) (mg/mmol) was assayed by ELISA-Albuwell kit (Exocell, Philadelphia, PA, USA) and normalised by urinary creatinine levels by Creatinine Companion ELISA kit (Exocell, Philadelphia, PA, USA) under the manufacturers' protocols [21, 23, 26]. The glucose concentration (mmol/l) in biological samples (plasma and urine) collected from terminated mice was measured by the glucose colorimetric kit (Cayman Chemical, Ann Arbor, MI, USA) [23].

Kidney pathology Periodic Acid Schiff (PAS) and Sirius Red staining of paraffin-embedded kidney sections was accomplished through standard protocols [27, 28]. Glomerulosclerosis and tubular injury (based on PAS images, semi-quantitative scale from 0 to 4) were assessed by a person blinded to the experimental group. The senescence-associated β-galactosidase assay (New England Biolabs [Canada], Whitby, ON, Canada) was performed in both frozen OCT-kidney sections and in the in vitro setting based upon the manufacturer's instructions. Semi-quantification of the relative staining in kidney sections was carried out in a blinded manner with the use of NIH Image J 1.51k software (http://rsb.info.nih.gov/ij/) [21, 27–29].

Real-time quantitative PCR Real-time quantitative PCR (RT-qPCR) was performed, using 7500 Fast real-time PCR system (Applied Biosystems, Mississauga, ON, Canada), in freshly isolated renal proximal tubules (RPTs) by the Percoll gradient method as reported previously [23, 27]. The mRNA change in each gene was determined and normalised to its own *Rpl13a* mRNA. Fold change in expression of target genes compared with the reference group was calculated using the $2^{-\Delta\Delta C_t}$ method. The primers used are shown in extra supplementary material (ESM) Table 1.

Immunohistochemical studies and reagents Western blotting (WB), immunohistochemistry (IHC) and immunofluorescence (IF) were performed using standard protocols as previously reported [21, 23, 26]. The antibodies used are listed in ESM Table 2.

KU-55933 (a specific ataxia-telangiectasia mutated [ATM] inhibitor) and AZD1390 (a selective ATM- and Rad3-related [ATR] kinase inhibitor) (www.selleckchem.com) are two Selleckchem products purchased via Cedarlane Laboratories (Burlington, ON, Canada), while canagliflozin (Invokana) (an SGLT2 inhibitor) was bought from Janssen (Toronto, ON, Canada).

Cell culture Primary mouse RPTC cultures were performed as reported previously [30, 31]. The mycoplasma-free HK-2 cell line (catalogue no. CRL-2190) was obtained from American Tissue Cell Collection (ATCC) (Manassas, VA, USA) (http://

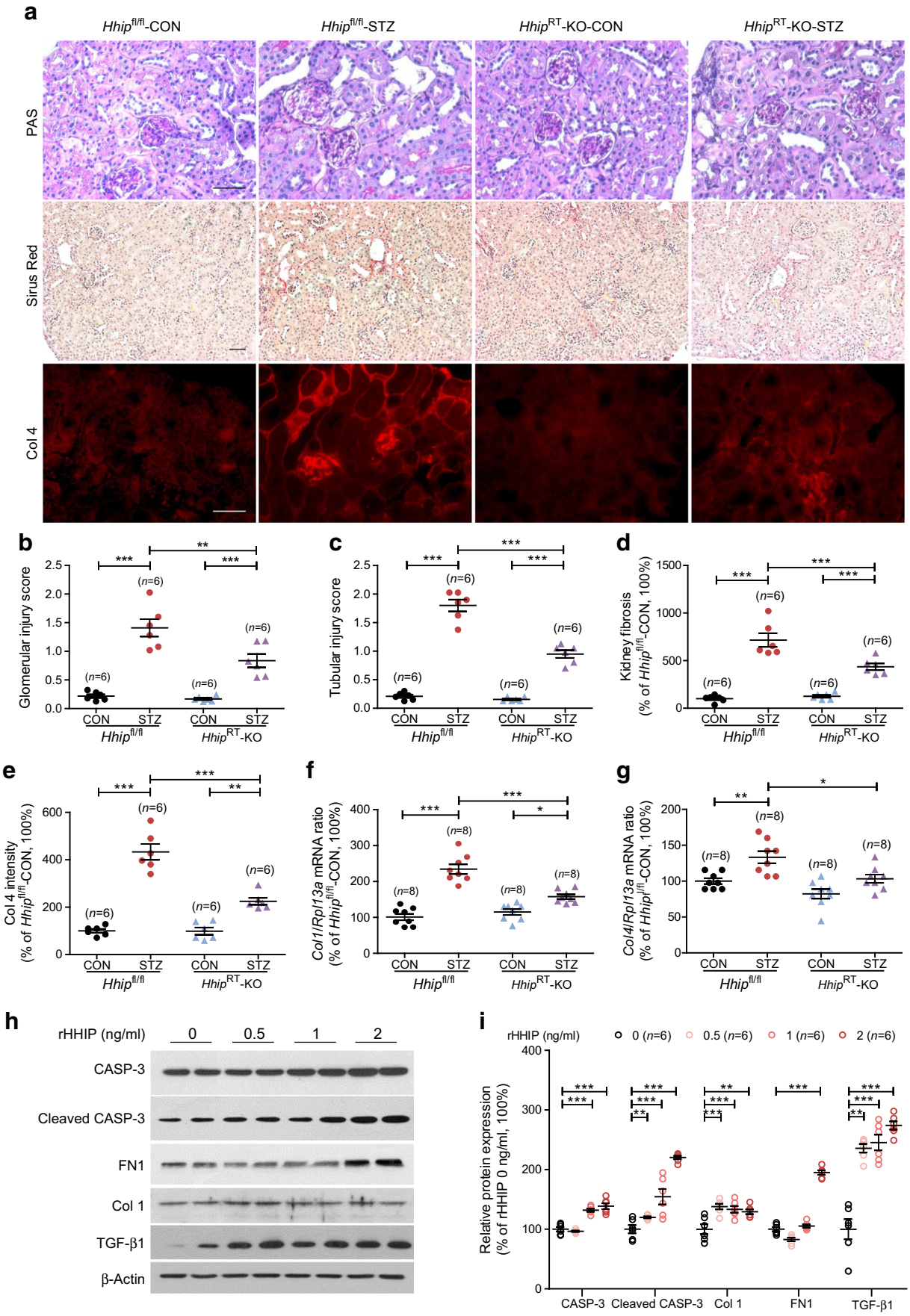
a
Hhip fl/fl-CON
Hhip fl/fl-STZ
Hhip RT-KO-CON
Hhip RT-KO-STZ
PAS
Sirus Red
Col 4
b
Glomerular injury score
c
Tubular injury score
d
Kidney fibrosis (% of Hhip fl/fl-CON, 100%)
e
Col 4 intensity (% of Hhip fl/fl-CON, 100%)
f
Col1/Rpl13a mRNA ratio (% of Hhip fl/fl-CON, 100%)
g
Col4/Rpl13a mRNA ratio (% of Hhip fl/fl-CON, 100%)
CON
STZ
Hhip fl/fl
Hhip RT-KO
h
rHHIP (ng/ml) 0 0.5 1 2
CASP-3
Cleaved CASP-3
FN1
Col 1
TGF-β1
β-Actin
i
rHHIP (ng/ml) 0 (n=6) 0.5 (n=6) 1 (n=6) 2 (n=6)
Relative protein expression (% of rHHIP 0 ng/ml, 100%)
CASP-3
Cleaved CASP-3
Col 1
FN1
TGF-β1

◀ **Fig. 4** DKD-related tubulopathy in vivo (**a**–**g**) and in vitro (**h**, **i**). (**a**) Representative images of PAS, Sirius Red and Col 4 IF staining in the kidneys of studied mice. Scale bar, 50 μm. (**b**, **c**) Semi-quantification of glomerular (**b**) and tubular (**c**) injury score (based on PAS images, semi-quantitative scale from 0 to 4). (**d**, **e**) Semi-quantification of tubulointerstitial fibrosis (**d**, Sirius Red staining; **e**, Col 4 IF staining). (**f**, **g**) *Col1* (**f**) and *Col4* (**g**) mRNA expression in isolated RPTs. mRNA change was determined and normalised to its own *Rpl13a* mRNA. (**h**, **i**) WB analysis on the relevant fibrotic (*Fn1*, *Col1* and *Tgfβ1*) and apoptotic (total and cleaved *Casp3*) genes in cells treated with rHHIP for 24 h. Representative immunoblots (**h**) are shown with semi-quantification of WB (**i**). Three separate experiments were performed. Data are shown as mean ± SEM for the indicated number of mice. *$p \leq 0.05$, **$p \leq 0.01$ and ***$p \leq 0.001$ (one-way ANOVA, followed by Bonferroni's post hoc test), CASP-3, caspase 3; Col 1/4, collagen I/IV

www.atcc.org). The plasmid, pcDNA3.1/mHhip (mouse) was a gift from A. McMahon (Harvard University, Cambridge, MA, USA) [12]. The transfection efficiency in HK2 cells was verified by transient transfection with a plasmid containing full-length pEGFP/mHhip (vs control plasmid, pEGFP N1; https://www.takarabio.com/) (ESM. Fig. 1a,b). HK2 cells were cultured in either normal (5 mmol/l D-glucose plus 30 mmol/l D-mannitol) or high D-glucose (35 mmol/l D-glucose) ± recombinant HHIP (rHHIP) or the relevant inhibitors. An HK2 stable clone containing human hSGLT2 gene promoter as reported previously [28] was tested by recombinant proteins (rTGF-β1 or rHHIP) (R&D Systems, Burlington, ON, Canada).

Cellular glucose uptake was assessed as 2-(*n*-[7-nitrobenz-2-oxa-1,3-diazol-4-yl]amino)-2-deoxyglucose (2-NBDG) (Invitrogen, Burlington, ON, Canada) entry into the cells as previously described [27]. The 2-NBDG fluorescence intensity was detected by BioTek fluorescence microplate reader with the filter of excitation 488 nm and emission 545 nm.

Statistical analysis For animal studies, groups of 6–12 mice were used. A power analysis based on the *t* test indicated that a sample size of 6 mice per group would be required to detect a statistically significant difference with a power of 80% (α=0.05). In vitro, three or four separate experiments were performed for each protocol. All values represent mean ± SEM. Statistical significance between the experimental groups was analysed by one-way ANOVA, followed by the Bonferroni test using Prism 6.0 software (GraphPad, San Diego, CA, USA). A probability level of $p \leq 0.05$ was considered to be statistically significant (*$p \leq 0.05$; **$p \leq 0.01$; ***$p \leq 0.001$) [21, 28, 29].

Results

A murine LDSTZ model in *Hhip*^{RT}-KO mice The *Hhip*^{RT}-KO mice (Fig. 1a shows genotyping; Fig. 1b shows WB of isolated RPTs; Fig. 1c shows IF staining) were generated by crossbreeding *Hhip*$^{fl/fl}$ mice and *Pax8*^{Cre} mice [22, 23]. Male mice with and without diabetes (*Hhip*$^{fl/fl}$ and *Hhip*^{RT}-KO) were studied from 10 weeks to 20 weeks of age. Diabetic mice weighed less than non-diabetic mice throughout the lifespan, regardless of whether they were HHIP deficient or not (Fig. 1d). Longitudinal SBP measurement (Fig. 1e) showed a similar pattern among the four subgroups of mice (non-diabetic vs diabetic; *Hhip*$^{fl/fl}$ vs *Hhip*^{RT}-KO). Compared with the respective non-diabetic control mice, random checks of blood glucose showed that hyperglycaemia was more pronounced in diabetic *Hhip*$^{fl/fl}$-STZ mice than in *Hhip*^{RT}-KO-STZ mice (Fig. 1f).

Ten weeks after the induction of diabetes, diabetic mice weighed less (ESM. Fig. 1c), had bigger kidneys (Fig. 1g, kidney weight/tibia length [KW/TL] ratio; ESM Fig. 1d, kidney weight/body weight [KW/BW] ratio), more pronounced glucosuria (mmol/l) (Fig. 1h) and hyperglycaemia (Fig. 1i), and increased UACR (Fig. 1j) when compared with non-diabetic mice, regardless of the presence or absence of HHIP deficiency. However, compared with diabetic *Hhip*$^{fl/fl}$-STZ mice, diabetic *Hhip*^{RT}-KO-STZ mice had significantly less pronounced hyperglycaemia (Fig. 1i) and decreased UACR (Fig. 1j), although the degree of glucosuria (Fig. 1h) was similar. Notably, GFR was only elevated in the kidneys of diabetic *Hhip*$^{fl/fl}$-STZ mice, and hyperfiltration was not evident in either of the non-diabetic control groups (*Hhip*$^{fl/fl}$-CON and *Hhip*^{RT}-KO-CON) or in the diabetic *Hhip*^{RT}-KO-STZ mice (Fig. 1k).

SGLT2 expression in renal tubular cells in vivo and in vitro We examined the expression of glucose transporters, including sodium–glucose cotransporter 1 (SGLT1), SGLT2 and GLUT2, which are responsible for glucose handling in RPTs [32]. Compared with the non-diabetic control mice, diabetic *Hhip*$^{fl/fl}$-STZ mice displayed significant elevation of *Sglt2* (also known as *Slc5a2*) mRNA in their RPTs (Fig. 2b), and this increased *Sglt2* expression was further confirmed by the co-localised IF staining of SGLT2 (Fig. 2d,e) and lotus tetragonolobus lectin (LTL, a marker of RPTs) (Fig. 2d,f) [27]. In contrast, diabetic *Hhip*^{RT}-KO-STZ mice had expression levels of *Sglt2* in their RPTs similar to those in non-diabetic control mice (*Hhip*$^{fl/fl}$-CON vs *Hhip*^{RT}-KO-CON) (qPCR, Fig. 2b; IF, Fig. 2d–f). There were no apparent differences in *Sglt1* (also known as *Slc5a1*) (qPCR, Fig. 2a) or

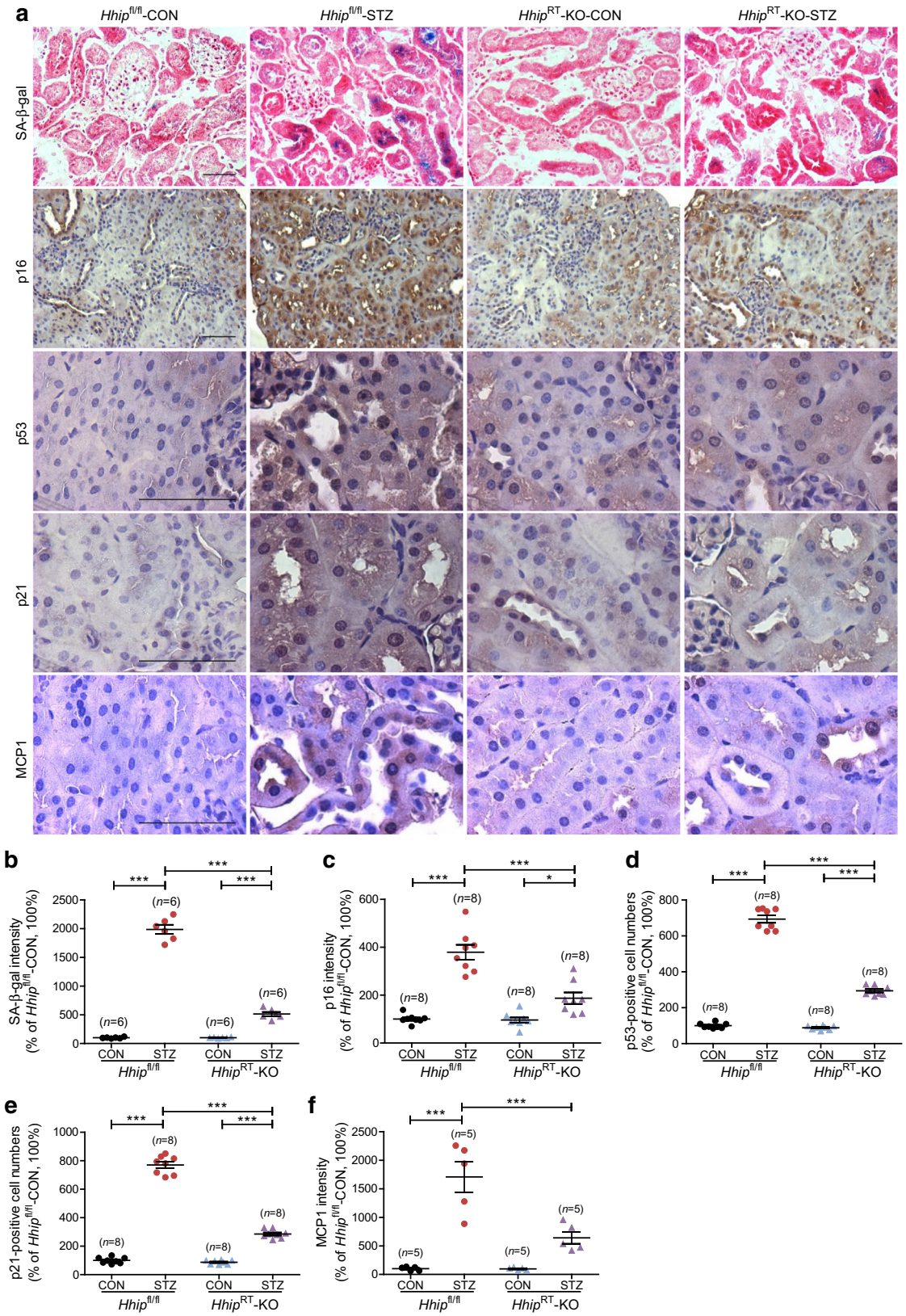

Fig. 5 Tubular cell senescence in vivo. (**a**) Representative IHC images of relevant staining (β-galactosidase and cellular senescence markers p16, p21, p53 and MCP1) in the kidneys of studied mice. Scale bar, 50 μm. (**b**–**f**) Semi-quantification of the relevant IF staining: β-galactosidase (**b**); p16 (**c**); p53 (**d**); p21 (**e**); and MCP1 (**f**). Data are shown as mean ± SEM for the indicated number of mice. *$p \leq 0.05$ and ***$p \leq 0.001$ (one-way ANOVA, followed by Bonferroni's post hoc test). SA-β-gal, senescence-associated β-galactosidase

Glut2 (also known as *Slc2a2*) expression in RPTs between any subgroups (qPCR, Fig. 2c; IF, Fig. 2g).

We next validated changes in *Sglt2* gene expression in vitro. In HK2 cells, high glucose (35 mmol/l vs 5 mmol/l D-glucose) increased SGLT2 protein expression, also noted in cells overexpressing mouse *Hhip* by transient transfection with the pcDNA3.1/mHhip plasmid (IF staining, Fig. 3a–c; WB, Fig. 3d and ESM Fig. 1e). This increased SGLT2 protein expression was particularly evident in cells exposed to a high-glucose milieu (Fig. 3a–d and ESM Fig. 1e). In addition, rHHIP dose-dependently activated SGLT2 protein expression (IF, Fig. 3e,f; WB, Fig. 3g and ESM Fig. 1f) and cellular glucose uptake activity (Fig. 3h,i); and this increased cellular glucose uptake activity was abolished by the administration of canagliflozin at 500 nmol/l (Fig. 3h,i). Furthermore, rTGF-β1 (from 0 to 0.5 ng/ml) dose-dependently stimulated hSGLT2 promoter activity at 6 and 12 h (ESM Fig. 2a,b), prior to the effect of rHHIP (from 0 to 2 ng/ml) on hSGLT2 promoter only at 12 h (ESM Fig. 2c,d) in HK2 cells.

DKD-induced tubulopathy in vivo and in vitro Kidney morphology displayed in the kidneys of adult *Hhip*^{RT}-KO-CON mice was indistinguishable from that in kidneys of *Hhip*$^{fl/fl}$-CON mice after PAS, Sirius Red and collagen IV (Col 4) IF staining (Fig. 4a). After 10 weeks of diabetes, *Hhip*$^{fl/fl}$-STZ mice developed nephropathy including tubulopathy (loss of brush border, detachment of tubular epithelial cells from tubular basement membrane, dilated tubules and tubulointerstitial fibrosis) (Fig. 4a–e). Tubulointerstitial fibrosis was further confirmed by *Col1* (also known as *Col1a1*) and *Col4* (also known as *Col4a1*) mRNA expression (Fig. 4f,g). In contrast, these RPTs abnormalities were significantly less prominent in the kidneys of diabetic *Hhip*^{RT}-KO-STZ mice (Fig. 4a–g).

In vitro, rHHIP directly stimulated the protein expression of fibrotic genes (fibronectin [*Fn1*], *Col1*, *Tgfβ1*) and apoptotic genes (total caspase 3 [*Casp3*] and cleaved *Casp3*) in a dose-dependent manner, as assessed by WB (Fig. 4h,i).

DKD-induced tubular cell senescence in vivo and in vitro We next examined senescence-associated β-galactosidase activity (Fig. 5a,b) and the expression of several cellular senescence markers (p16, p21, p53 and monocyte chemoattractant protein-1 [MCP1] assessed by IHC in the different groups of mice (Fig. 5a–f). There was no apparent difference in those variables when comparing non-diabetic mouse groups (*Hhip*$^{fl/fl}$-CON vs *Hhip*^{RT}-KO-CON). The diabetic *Hhip*$^{fl/fl}$-STZ mice developed apparent tubular senescence, assessed by senescence-associated β-galactosidase activity, accompanied by an increase in the expression of certain senescence markers (p16, p21, p53 and MCP1) in their RPTs. In contrast, this elevated tubular senescence was significantly attenuated in the RPTs of diabetic *Hhip*^{RT}-KO-STZ mice (Fig. 5).

In HK2 cells, high glucose (35 mmol/l D-glucose) directly stimulated mRNA expression of *HHIP* and senescence markers *P16* (also known as *CDKN2A*), *P21* (*CDKN1A*) and *P53* (*TRP53*) (Fig. 6a). As compared with the cells transfected by pcDNA3.1 control plasmid (1 μg/μl), the cells overexpressing mouse HHIP (pcDNA3.1/mHhip, 1 μg/μl) displayed increased cellular senescence, with the number of positive senescent cells being markedly pronounced in cells exposed to a milieu of 35 mmol/l (vs 5 mmol/l) D-glucose (Fig. 6b,c). Similarly, rHHIP triggered senescence-associated β-galactosidase activity in a dose-dependent manner (Fig. 6d,e).

Moreover, overexpression of mouse HHIP (pcDNA3.1/mHhip, 1 μg/μl) (Fig. 6f,g) directly increased SGLT2 protein expression (Fig. 6f and ESM Fig. 2e) and greatly upregulated the mRNA expression of several cellular senescence markers (p16, p21 and p53) (Fig. 6h) and inflammatory cytokines (*IL6*, *IL1β* and *MCP1* [also known as *CCL2*]) (Fig. 6i). We further confirmed that canagliflozin (500 nmol/l) inhibited rHHIP (2 ng/ml)-triggered senescence-associated β-galactosidase activity in primary RPTCs from *Hhip*$^{fl/fl}$ mice (Fig. 6j,k).

In mammalian cells, ATM and ATR kinase are the central regulators for cell-cycle arrest [33]. In HK2 cells, we found that rHHIP (2ng/ml) apparently triggered senescence-associated β-galactosidase activity, which was inhibited by the administration of both ATM and ATR inhibitors (Fig. 7a,b). In addition, IF analysis showed that rHHIP (2 ng/ml) inhibited CDK1 (Fig. 7c,d) and CDK2 (Fig. 7e,f) expression; this inhibitory effect was prevented by the administration of both ATM and ATR inhibitors (Fig. 7c–f).

Cellular senescence in *Hhip*^{RPTC}-Tg mice We generated *Hhip*^{RPTC}-Tg mice by overexpressing mouse *Hhip* in their RPTCs (Fig. 8a–g and ESM Fig. 3). We confirmed that compared with non-Tg littermates, *Hhip*^{RPTC}-Tg mice overexpressed Myc-mHhip-Flag mRNA in the kidneys and in isolated RPTs (ESM Fig. 3a,b). These findings were confirmed by co-localised staining of HHIP and aquaporin 1 (a marker of RPTs) (Fig. 8a). Adult *Hhip*^{RPTC}-Tg mice at age 20 weeks were phenotypically indistinguishable from non-Tg littermates, including monitored hyperglycaemia (Fig. 8b) and measured GFR (Fig. 8c). Intriguingly, compared with non-Tg littermates, *Hhip*^{RPTC}-Tg mice displayed increased SGLT2 expression (co-localised with LTL) (Fig. 8d–f) and heightened

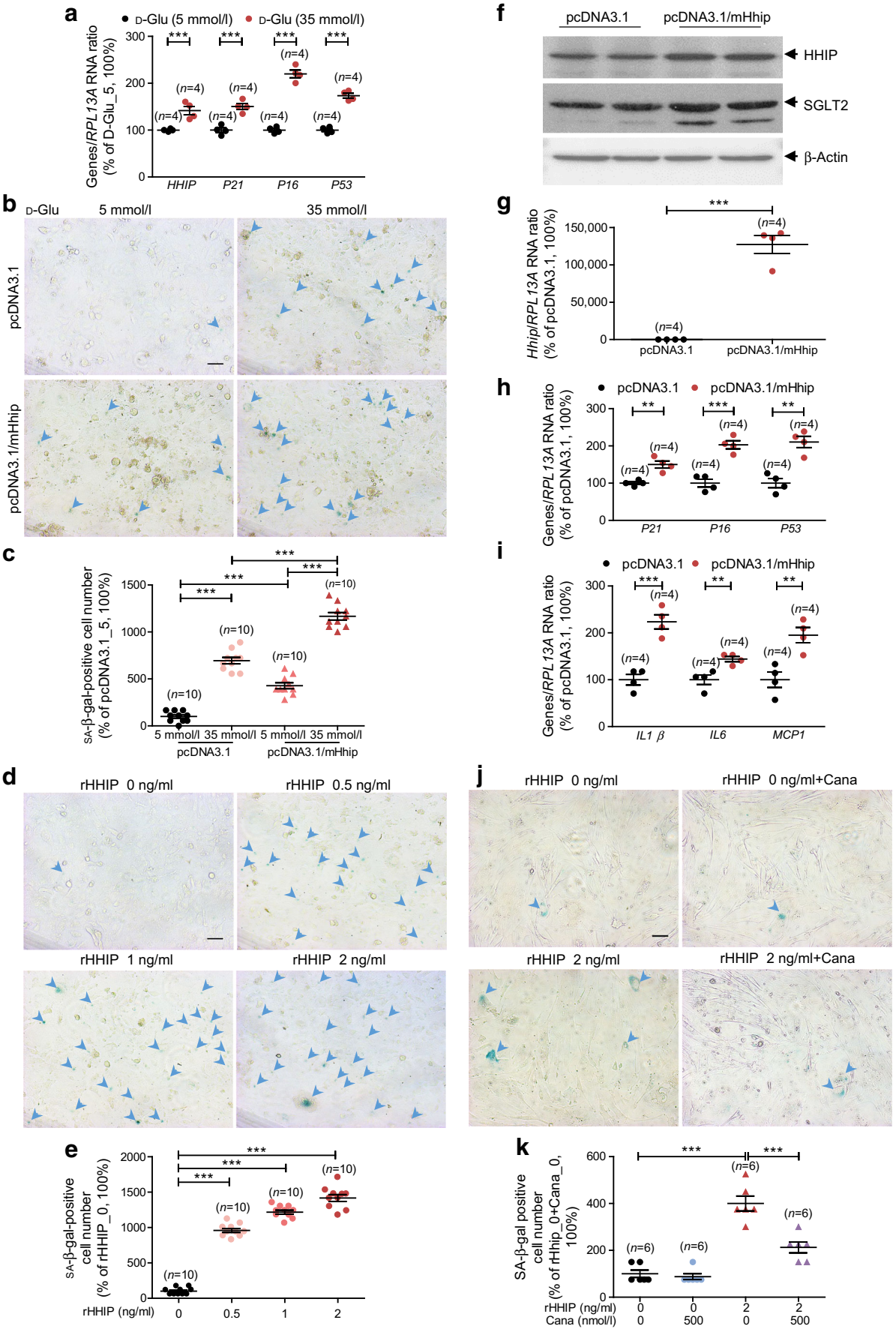
a
D-Glu (5 mmol/l)
D-Glu (35 mmol/l)
Genes/RPL13A RNA ratio (% of D-Glu_5, 100%)
HHIP
P21
P16
P53
b
D-Glu
5 mmol/l
35 mmol/l
pcDNA3.1
pcDNA3.1/mHhip
c
SA-β-gal-positive cell number (% of pcDNA3.1_5, 100%)
5 mmol/l 35 mmol/l 5 mmol/l 35 mmol/l
pcDNA3.1
pcDNA3.1/mHhip
d
rHHIP 0 ng/ml
rHHIP 0.5 ng/ml
rHHIP 1 ng/ml
rHHIP 2 ng/ml
e
SA-β-gal-positive cell number (% of rHHIP_0, 100%)
rHHIP (ng/ml)
f
pcDNA3.1
pcDNA3.1/mHhip
HHIP
SGLT2
β-Actin
g
Hhip/RPL13A RNA ratio (% of pcDNA3.1, 100%)
h
Genes/RPL13A RNA ratio (% of pcDNA3.1, 100%)
i
IL1 β
IL6
MCP1
j
rHHIP 0 ng/ml
rHHIP 0 ng/ml+Cana
rHHIP 2 ng/ml
rHHIP 2 ng/ml+Cana
k
SA-β-gal positive cell number (% of rHhip_0+Cana_0, 100%)
rHHIP (ng/ml)
Cana (nmol/l)

◀ **Fig. 6** Tubular cell senescence in vitro. (**a**) qPCR analysis in HK2 cells exposed to 5 mmol/l or 35 mmol/l D-glucose for 24 h. Four separate experiments were performed. (**b**–**e**) β-galactosidase staining in HK2 cells. HK2 cells overexpressing mouse HHIP were treated with either 5 mmol/l or 35 mmol/l D-glucose for 24 h (**b**, **c**). HK2 cells were treated with rHHIP dose-dependently for 24 h (**d**, **e**). Representative images are shown (**b**, **d**), together with semi-quantification of β-galactosidase staining (**c**, **e**). Scale bar, 50 μm. Three separate experiments (triplicated setting for each experiment) were performed. (**f**) WB analysis in HK2 cells overexpressing mouse HHIP. Three separate experiments were performed. (**g**–**i**) qPCR analysis of expression of mouse *Hhip* mRNA (**g**), cellular senescence marker mRNA (*P16*, *P21* and *P53*) (**h**) and inflammatory cytokine (mRNA *IL1β*, *IL6* and *MCP1*) (**i**). Four separate experiments were performed. (**j**, **k**) β-galactosidase staining in primary RPTCs from $Hhip^{fl/fl}$ mice treated with rHHIP ± canagliflozin. Representative images are shown (**j**), together with semi-quantification (**k**). Scale bar, 50 μm. Three separate experiments (duplicated setting per each experiment) were performed. Data are shown as mean ± SEM for the indicated number of mice. $^{**}p \leq 0.01$ and $^{***}p \leq 0.001$ (one-way ANOVA, followed by Bonferroni's post hoc test). Cana, canagliflozin; Cana_0, canagliflozin 0 nmol/l; D-Glu, D-glucose; pcDNA3.1_5, pcDNA3.1 at 5 mmol/l D-glucose; rHHIP_0, rHHIP 0 ng/ml; SA-β-gal, senescence-associated β-galactosidase

SASP including β-galactosidase activity and cellular senescence markers (p16, p21 and p53) (Fig. 8g and ESM Fig. 3c–f) in their RPTs. In addition, as compared with $Hhip^{fl/fl}$ mice, the heightened β-galactosidase activity was evident in primary RPTCs from $Hhip^{RPTC}$-Tg mice (ESM Fig. 3g,h) and was inhibited by the administration of canagliflozin (500 nmol/l) (ESM Fig. 3g,h).

Discussion

In the present study, we demonstrated that renal tubule-specific HHIP deficiency protected mice from the development of DKD tubulopathy. The study showed that high-glucose-induced HHIP expression/secretion stimulated *Sglt2* gene expression, which further increased intracellular glucose concentration. In parallel, this increased HHIP expression exacerbated cellular senescence by releasing inflammatory cytokines in RPTs. Both actions formed a vicious cycle, ultimately leading to DKD tubulopathy. In contrast, renal tubule-specific HHIP deficiency attenuated these changes, thereby protecting the kidney. The hypothetical process by which this may occur is depicted schematically in Fig. 8h.

There is a growing body of literature that demonstrates the importance of tubular function in regulating glomerular filtration and glucose reabsorption in the context of diabetes [4]. The renal tubular epithelium is a key participant in a sequence of cellular events from adaptive (hypertrophy) to maladaptive (dedifferentiation, EMT, apoptosis and/or fibrosis) as a response to kidney injury in diabetes [4]. We have systematically studied and reported that hyperglycaemia stimulated renal HHIP expression in diabetic kidneys (i.e. glomerulus, tubule, urinary casts and urine) in both humans [20] and diabetic mice [21]. Our data showed that HHIP is involved in the development of diabetic nephropathy. Here, with the aid of our recently generated renal tubule-specific *Hhip* deletion and overexpression mouse lines ($Hhip^{RT}$-KO and $Hhip^{RPTC}$-Tg mice), we aimed to study the role of renal tubule HHIP in DKD tubulopathy.

As recommended by the NIH Animal Models of Diabetic Complications Consortium, LDSTZ eliminates or minimises potential STZ nephrotoxicity [34]. LDSTZ-induced diabetic mice show the development of albuminuria and increased GFR but no hypertension; these DKD features are more pronounced in male than in female C57BL/6 mice [35, 36]. Notably, the adult $Hhip^{RT}$-KO mice are phenotypically indistinguishable from $Hhip^{fl/fl}$ mice (male or female), making the LDSTZ-induced murine diabetic model ideal by excluding the impact of STZ destruction of pancreatic beta cells, as we showed the functional link of HHIP to pancreatic beta cell dysfunction [37]. Here, we conducted all experiments in male mice ($Hhip^{RT}$-KO vs $Hhip^{fl/fl}$) rendered diabetic for a period of 10 weeks. As previously reported [24, 38, 39], features of LDSTZ-DKD, such as elevated blood glucose levels, increased GFR and UACR, and overall DKD degenerative pathologies including tubulopathy, occurred in diabetic $Hhip^{fl/fl}$-STZ mice. In contrast, those changes were substantially attenuated in diabetic $Hhip^{RT}$-KO-STZ. There was no hypertensive phenotype involved in the current model.

$Hhip^{fl/fl}$-CON and $Hhip^{RT}$-KO-CON mice had similar basal expression levels of *Sglt1*, *Sglt2* and *Glut2*. However, lower *Sglt2* IF expression was evident in the RPTs of diabetic $Hhip^{RT}$-KO-STZ (vs $Hhip^{fl/fl}$-STZ) mice, while *Sglt1* and *Glut2* expression remained unchanged, suggesting a functional interaction between HHIP and SGLT2 in RPTs in the presence of diabetes. In diabetes, excessive glucose uptake via SGLT2 (mediating more than 90% of glucose resorption [40]) may contribute to glucose toxicity, hyperfiltration and glomerular injury, as well as to proinflammatory cytokine production [10]. Indeed, the cardio- and reno-protective effects of SGLT2 inhibitors have now been documented in large clinical trials in individuals with type 2 diabetes [3, 41–44]. We did not observe apparent changes in either SGLT1 and GLUT2 expression (mRNA and protein) in our model, although studies in rats and mice with STZ-induced

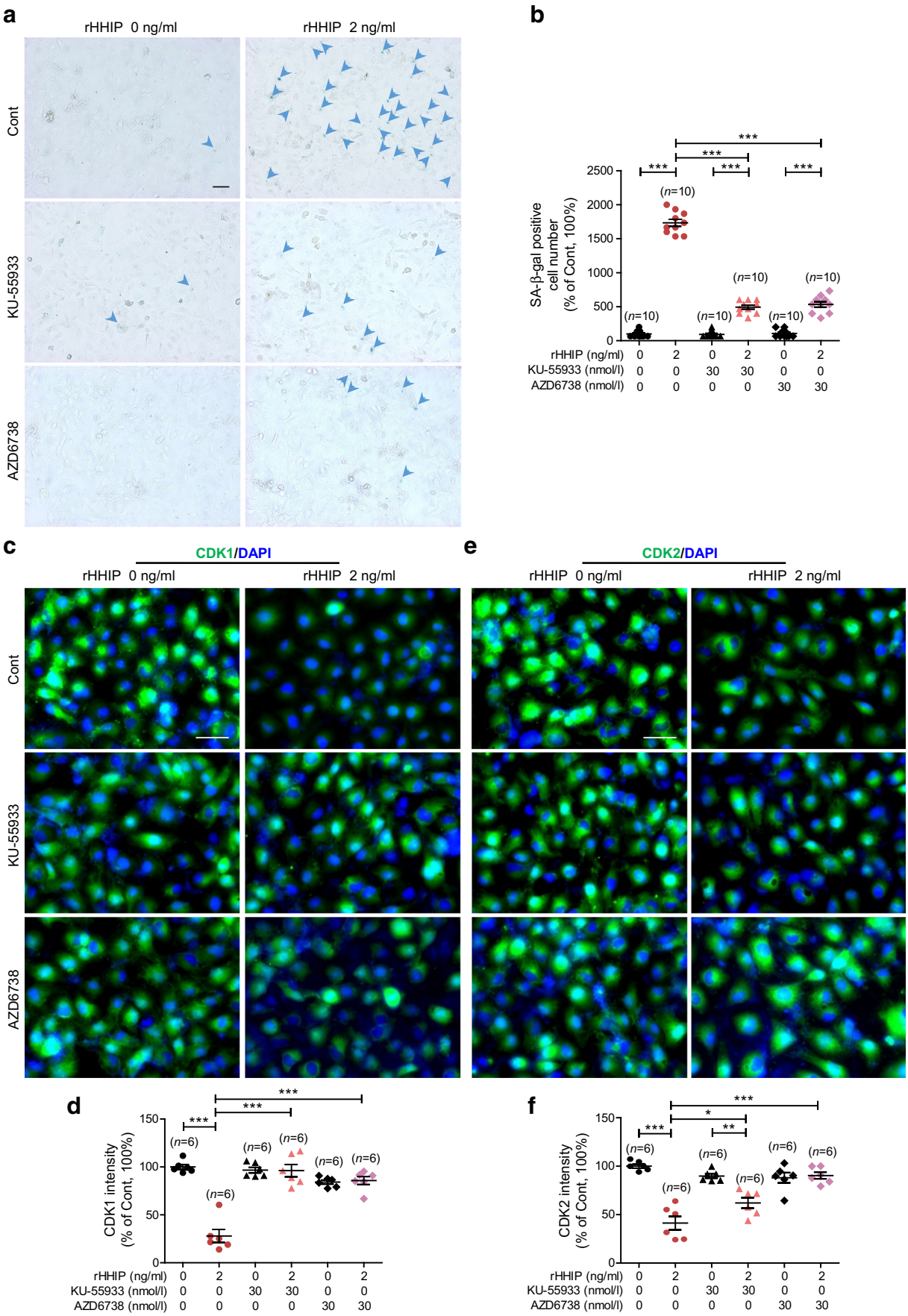
a
rHHIP 0 ng/ml
rHHIP 2 ng/ml
Cont
KU-55933
AZD6738
b
SA-β-gal positive cell number (% of Cont, 100%)
rHHIP (ng/ml)
KU-55933 (nmol/l)
AZD6738 (nmol/l)
c
CDK1/DAPI
e
CDK2/DAPI
d
CDK1 intensity (% of Cont, 100%)
f
CDK2 intensity (% of Cont, 100%)

◀ **Fig. 7** ATM- and ATR-mediated cell arrest in HK2 cells. HK2 cells were treated with rHHIP ± ATM inhibitor (KU-55933) or ATR inhibitor (AZD6738) for 24 h. (**a**, **b**) Representative images of β-galactosidase staining are shown (positive SA-β-gal staining indicated by arrowheads) (**a**), together with semi-quantification of staining (**b**). Scale bar, 50 μm. Three separate experiments (triplicated setting for each experiment) were performed. (**c**–**f**) Representative images of CDK1 (**c**) and CDK2 (**e**) staining are shown (CDK1, green; CDK2, green; DAPI, blue) staining are shown, together with semi-quantification of staining (**d**, CDK1; **f**, CDK2). Scale bar, 50 μm. Three separate experiments (duplicated setting per each experiment) were performed. Data are shown as mean ± SEM for the indicated numbers of mice. $*p \leq 0.05$, $**p \leq 0.01$ and $***p \leq 0.001$ (one-way ANOVA, followed by Bonferroni's post hoc test). Cont, no treatment; SA-β-gal, senescence-associated β-galactosidase

diabetes have indicated a concerted upregulation of luminal and basolateral GLUT2 facilitating diffusion in contribution of glucose reabsorption in RPTs [45–47].

In HK2 cells, both HHIP overexpression or treatment with rHHIP directly stimulated SGLT2 protein expression and activity, and those elevations were further pronounced in cells exposed to high-glucose milieu. With these results, we concluded that the glucose-lowering property observed in diabetic *Hhip*^{RT}-KO-STZ (vs diabetic *Hhip*$^{fl/fl}$-STZ) mice might be due to lower SGLT2 expression in their RPTs. Therefore, diabetic *Hhip*^{RT}-KO-STZ mice displayed glucosuria much like diabetic *Hhip*$^{fl/fl}$-STZ mice. Multiple factors/pathways have been involved in the regulation of *Sglt2* gene expression/activity in DKD [5]. Among these pathways, it is known that TGF-β1, via phosphorylated Smad3, increases SGLT2 expression in HK2 cells [48, 49]. Previously, we demonstrated that HHIP stimulated TGF-β1 promoter activity, protein expression and TGFβ1–Smad2/3 cascade signal, mediating cellular remodelling in both non-diabetic [29] and diabetic settings [21]. Our present data demonstrated that rTGF-β1-stimulated hSGLT2 promoter activity takes place prior to the effect of rHHIP on hSGLT2 promoter, suggesting that the HHIP-induced increase in SGLT2 expression may be mediated via TGF-β1. Future studies will be needed to identify the exact mechanism.

SGLT2 inhibition, counteracting the diabetes-induced production of proinflammatory cytokines, plays a key role in kidney-protective effects [5, 50]. An increase in senescent cells in DKD and the senescent tubular epithelial cell appears to be an appealing target linked to DKD-related tubulopathy [8, 9, 50]. Previously, we demonstrated that excessive urinary HHIP production and the release of a variety of inflammatory cytokines in both diabetic human and mouse kidneys [20] underscore the occurrence of SASP. Here, we aimed to investigate the molecular basis of how RPTC HHIP promotes SASP, thereby advancing DKD-related tubulopathy.

In the present study, the senescence-associated β-galactosidase activity and gene expression of several SASP markers (p16, p21 and p53) were significantly elevated in the RPTs of diabetic *Hhip*$^{fl/fl}$ mice. In contrast, those SASP changes were either inhibited or attenuated in the RPTs of diabetic *Hhip*^{RT}-KO-STZ mice, underscoring the importance of localised HHIP deficiency in decreasing RPT's senescence in the context of diabetes. In vitro, overexpression of HHIP and treatment with rHHIP directly triggered SASP in HK2 cells, and this increased SASP was more pronounced in cells exposed to high-glucose milieu. Together, these data highlight the possible role of RPTC HHIP in cellular senescence. Indeed, compared with non-Tg littermates, *Hhip*^{RPTC}-Tg mice displayed higher expression levels of SGLT2 and increased senescence activity in their RPTCs at the basal level, and their increased β-galactosidase activity was inhibited by canagliflozin in primary RPTCs as well.

In mammalian cells, cellular responses to DNA damage are coordinated primarily by two distinct kinase signalling cascades, the ATM and ATR pathways, which are activated by DNA double-strand breaks and single-stranded DNA, respectively [33]. Both kinases rapidly phosphorylate p53 upon DNA damage, leading to the induction of p21^{Cip1}, to inhibit CDKs. In addition to p53, p16^{Ink4a} also leads to cell-cycle arrest via the inhibition of CDK4/CDK6 [10]. To ensure cell integrity after cellular senescence mediated by p53-p21^{Cip1} or p16^{Ink4a}, DNA is checked during cell-cycle progression in the G1/S or G2/M phases, a machinery process [9, 10]. As shown in the simplified version of the ATM and ATR signalling map (https://www.selleckchem.com/atm.html), ATM-CDK2 appears to mainly target the G1/S phase, while ATR-CDK1 targets the G2/M phase. Here, our in vitro data revealed that both ATM and ATR inhibitors abolished the rHHIP-induced cellular senescence, underscoring the arrest of the G1/S or G2/M caused by HHIP-SASP in the context of diabetes. However, the operation of ATM/ATR machinery process in detail merits study.

In conclusion, our data suggest that, in the context of diabetes, HHIP deficiency in renal tubular cells prevents DKD tubulopathy, possibly by inhibition of *Sglt2* gene expression to maintain normal glucose haemodynamics and by inhibition of cellular senescence to eliminate proinflammatory cytokine production, a novel finding.

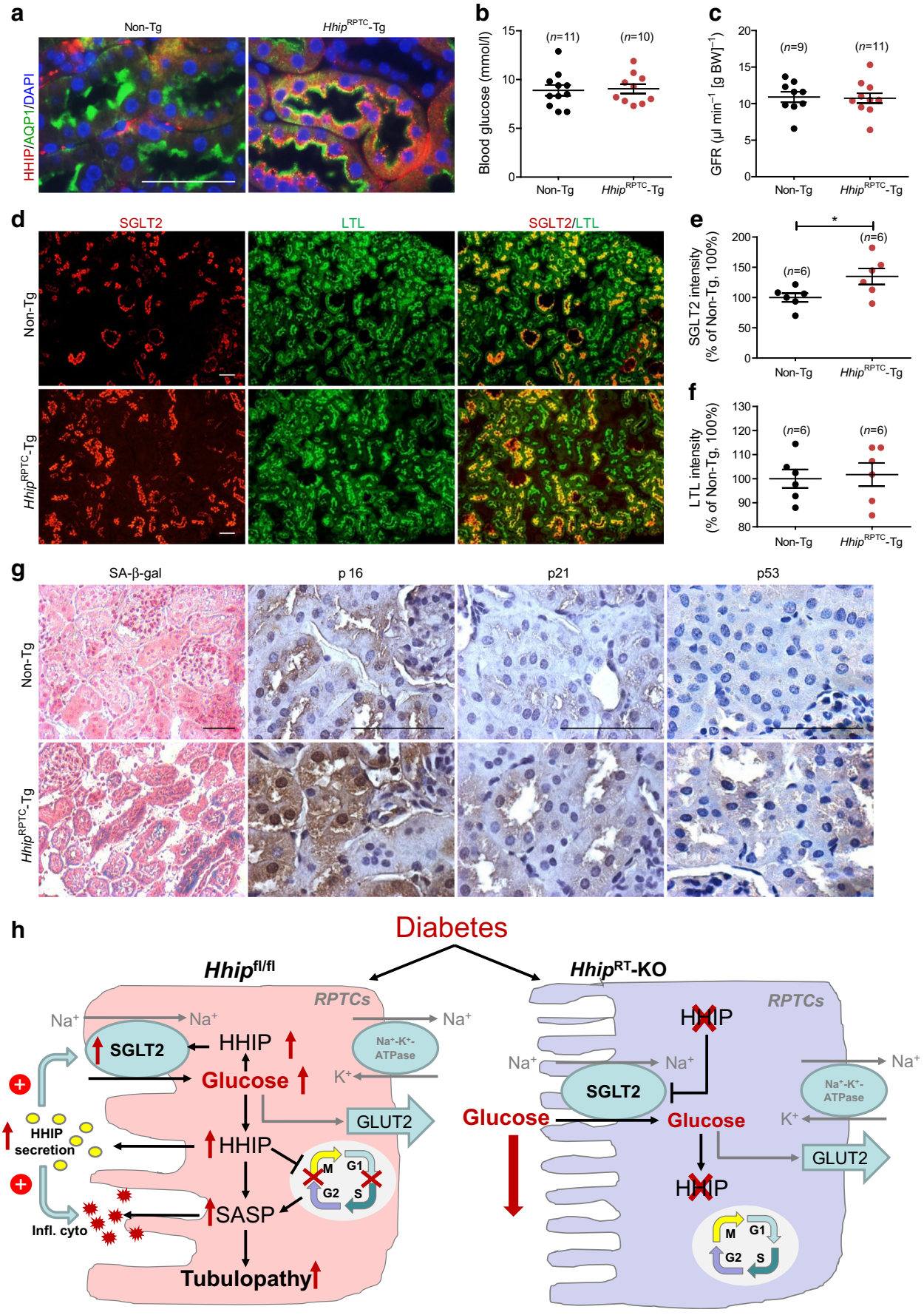
a
Non-Tg
Hhip^RPTC-Tg
HHIP/AQP1/DAPI
b
Blood glucose (mmol/l)
(n=11)
(n=10)
Non-Tg
Hhip^RPTC-Tg
c
GFR (μl min−1 [g BW]−1)
(n=9)
(n=11)
d
SGLT2
LTL
SGLT2/LTL
e
SGLT2 intensity (% of Non-Tg, 100%)
(n=6)
(n=6)
f
LTL intensity (% of Non-Tg, 100%)
(n=6)
(n=6)
g
SA-β-gal
p 16
p21
p53
h
Diabetes
Hhip^fl/fl
Hhip^RT-KO
RPTCs
Na+
SGLT2
HHIP
Glucose
Na+-K+-ATPase
K+
GLUT2
HHIP secretion
SASP
Infl. cyto
Tubulopathy
M
G1
G2
S

◀ **Fig. 8** (**a**–**g**) Kidney analysis in male *Hhip*^{RPTC}-Tg (vs non-Tg) mice at 20 weeks of age. Representative IF images of co-staining of kidney sections for HHIP (red), AQP1 (green) and DAPI (blue) are shown (**a**). Blood glucose was monitored by an Accu-Chek Performa glucose meter (**b**) and GFR was measured (**c**). Representative IF images of co-staining of kidney sections for SGLT2 (red) and LTL (green) are shown (**d**), together with semi-quantification of staining (**e**, **f**). Data are shown as mean ± SEM for the indicated numbers of mice. *$p \leq 0.05$ (one-way ANOVA, followed by Bonferroni's post hoc test). Representative IHC images of staining for β-galactosidase and several cellular senescence markers (p16, p21 and p53) are shown (**g**). Scale bar, 50 μm. (**h**) A schematic illustration of how HHIP deficiency in renal tubular cells mediates a concerted effect by restoring *Sglt2* gene expression to maintain glucose reabsorption, limiting cellular senescence to ameliorate renal haemodynamics, and inhibiting proinflammatory cytokine production, in the context of diabetes. AQP1, aquaporin 1; Infl. cyto, inflammatory cytokines; G1, cell cycle G1 phase; G2, cell cycle G2 phase; M, cell cycle mitosis phase; Na^+-K^+-ATPase, sodium/potassium-transporting ATPase; S, cell cycle synthesis phase; SA-β-gal, senescence-associated β-galactosidase

Supplementary Information The online version contains peer-reviewed but unedited supplementary material available at https://doi.org/10.1007/s00125-022-05810-6.

Data availability All data generated or analysed during this study are included in this published article (and its ESM).

Funding This project was supported by grants from the Canadian Institutes of Health Research (CIHR PJT173512 and PJT173534 to SLZ; CIHR MOP142378 to JSDC), The Natural Sciences and Engineering Research Council of Canada (NSERC, RGPIN-2017-05615 to SLZ) and Kidney Foundation of Canada (KFOC160019 to SLZ and KFOC 856016-21KHRG to JSDC).

Authors' relationships and activities The authors declare that there are no relationships or activities that might bias, or be perceived to bias, their work.

Contribution statement All authors made substantial contributions to the conception and design of the study and to the acquisition or analysis and interpretation of data. SLZ prepared the original draft of the manuscript and all authors critically revised it for important intellectual content. All authors accepted the final version to be published. SLZ is responsible for the integrity of the work as a whole.

References

1. Saran R, Li Y, Robinson B et al (2016) US renal data system 2015 annual data report: epidemiology of kidney disease in the United States. Am J Kidney Dis Off J Natl Kidney Foundation 67:Svii, S1-305. https://doi.org/10.1053/j.ajkd.2015.12.014
2. Schnell O, Valensi P, Standl E, Ceriello A (2020) Comparison of mechanisms and transferability of outcomes of SGLT2 inhibition between type 1 and type 2 diabetes. Endocrinol Diabetes Metab 3: e00129. https://doi.org/10.1002/edm2.129
3. Bhattarai M, Salih M, Regmi M et al (2022) Association of sodium-glucose cotransporter 2 inhibitors with cardiovascular outcomes in patients with type 2 diabetes and other risk factors for cardiovascular disease: a meta-analysis. JAMA Netw Open 5:e2142078. https://doi.org/10.1001/jamanetworkopen.2021.42078
4. Vallon V, Thomson SC (2020) The tubular hypothesis of nephron filtration and diabetic kidney disease. Nat Rev Nephrol 16:317–336. https://doi.org/10.1038/s41581-020-0256-y
5. Vallon V, Verma S (2021) Effects of SGLT2 inhibitors on kidney and cardiovascular function. Ann Rev Physiol 83:503–528. https://doi.org/10.1146/annurev-physiol-031620-095920
6. Ovadya Y, Krizhanovsky V (2015) A new twist in kidney fibrosis. Nat Med 21:975–977. https://doi.org/10.1038/nm.3938
7. Huang S, Susztak K (2016) Epithelial plasticity versus EMT in kidney fibrosis. Trends Mol Med 22:4–6. https://doi.org/10.1016/j.molmed.2015.11.009
8. Docherty MH, O'Sullivan ED, Bonventre JV, Ferenbach DA (2019) Cellular Senescence in the Kidney. J Am Soc Nephrol 30: 726–736. https://doi.org/10.1681/ASN.2018121251
9. Wiley CD (2020) Role of senescent renal cells in pathophysiology of diabetic kidney disease. Curr Diabetes Rep 20:33. https://doi.org/10.1007/s11892-020-01314-y
10. Xu J, Zhou L, Liu Y (2020) Cellular senescence in kidney fibrosis: pathologic significance and therapeutic strategies. Front Pharmacol 11:601325. https://doi.org/10.3389/fphar.2020.601325
11. Bosanac I, Maun HR, Scales SJ et al (2009) The structure of SHH in complex with HHIP reveals a recognition role for the Shh pseudo active site in signaling. Nat Struct Mol Biol 16:691–697. https://doi.org/10.1038/nsmb.1632
12. Chuang PT, McMahon AP (1999) Vertebrate hedgehog signalling modulated by induction of a hedgehog-binding protein. Nature 397: 617–621. https://doi.org/10.1038/17611
13. Kwong L, Bijlsma MF, Roelink H (2014) Shh-mediated degradation of Hhip allows cell autonomous and non-cell autonomous Shh signalling. Nat Commun 5:4849. https://doi.org/10.1038/ncomms5849
14. Lao T, Glass K, Qiu W et al (2015) Haploinsufficiency of Hedgehog interacting protein causes increased emphysema induced by cigarette smoke through network rewiring. Genome Med 7:12. https://doi.org/10.1186/s13073-015-0137-3
15. Lao T, Jiang Z, Yun J et al (2016) Hhip haploinsufficiency sensitizes mice to age-related emphysema. Proc Natl Acad Sci USA 113: E4681–E4687. https://doi.org/10.1073/pnas.1602342113
16. Kawahira H, Ma NH, Tzanakakis ES, McMahon AP, Chuang PT, Hebrok M (2003) Combined activities of hedgehog signaling inhibitors regulate pancreas development. Development (Cambridge, England) 130:4871–4879. https://doi.org/10.1242/dev.00653
17. Kayed H, Kleeff J, Esposito I et al (2005) Localization of the human hedgehog-interacting protein (Hip) in the normal and diseased pancreas. Mol Carcinog 42:183–192. https://doi.org/10.1002/mc.20088
18. Zhou X, Baron RM, Hardin M et al (2012) Identification of a chronic obstructive pulmonary disease genetic determinant that regulates HHIP. Hum Mol Genet 21:1325–1335. https://doi.org/10.1093/hmg/ddr569
19. Olsen CL, Hsu PP, Glienke J, Rubanyi GM, Brooks AR (2004) Hedgehog-interacting protein is highly expressed in endothelial cells but down-regulated during angiogenesis and in several human tumors. BMC Cancer 4:43. https://doi.org/10.1186/1471-2407-4-43
20. Miyata KN, Zhao XP, Chang SY et al (2020) Increased urinary excretion of hedgehog interacting protein (uHhip) in early diabetic kidney disease. Transl Res J Lab Clin Med 217:1–10. https://doi.org/10.1016/j.trsl.2019.11.001
21. Zhao XP, Chang SY, Liao MC et al (2018) Hedgehog interacting protein promotes fibrosis and apoptosis in glomerular endothelial cells in murine diabetes. Sci Rep 8:5958. https://doi.org/10.1038/s41598-018-24220-6

22. Bouchard M, Souabni A, Busslinger M (2004) Tissue-specific expression of cre recombinase from the Pax8 locus. Genesis (New York, NY : 2000) 38:105–109. https://doi.org/10.1002/gene.20008
23. Lo CS, Miyata KN, Zhao S et al (2019) Tubular deficiency of heterogeneous nuclear ribonucleoprotein F elevates systolic blood pressure and induces glycosuria in mice. Sci Rep 9:15765. https://doi.org/10.1038/s41598-019-52323-1
24. Brezniceanu ML, Liu F, Wei CC et al (2007) Catalase overexpression attenuates angiotensinogen expression and apoptosis in diabetic mice. Kidney Int 71:912–923. https://doi.org/10.1038/sj.ki.5002188
25. Lo CS, Shi Y, Chang SY et al (2015) Overexpression of heterogeneous nuclear ribonucleoprotein F stimulates renal Ace-2 gene expression and prevents TGF-beta1-induced kidney injury in a mouse model of diabetes. Diabetologia 58:2443–2454. https://doi.org/10.1007/s00125-015-3700-y
26. Miyata KN, Zhao S, Wu CH et al (2020) Comparison of the effects of insulin and SGLT2 inhibitor on the Renal Renin-Angiotensin system in type 1 diabetes mice. Diabetes Res Clin Pract 162:108107. https://doi.org/10.1016/j.diabres.2020.108107
27. Miyata KN, Lo CS, Zhao S et al (2021) Angiotensin II up-regulates sodium-glucose co-transporter 2 expression and SGLT2 inhibitor attenuates Ang II-induced hypertensive renal injury in mice. Clin Sci (London, England : 1979) 135:943–961. https://doi.org/10.1042/CS20210094
28. Zhao S, Lo CS, Miyata KN et al (2021) Overexpression of Nrf2 in renal proximal tubular cells stimulates sodium-glucose cotransporter 2 expression and exacerbates dysglycemia and kidney injury in diabetic mice. Diabetes 70:1388–1403. https://doi.org/10.2337/db20-1126
29. Liao MC, Zhao XP, Chang SY et al (2017) AT(2) R deficiency mediated podocyte loss via activation of ectopic hedgehog interacting protein (Hhip) gene expression. J Pathol 243:279–293. https://doi.org/10.1002/path.4946
30. Brezniceanu ML, Wei CC, Zhang SL et al (2006) Transforming growth factor-beta 1 stimulates angiotensinogen gene expression in kidney proximal tubular cells. Kidney Int 69:1977–1985. https://doi.org/10.1038/sj.ki.5000396
31. Zhang SL, Chen X, Hsieh TJ et al (2002) Hyperglycemia induces insulin resistance on angiotensinogen gene expression in diabetic rat kidney proximal tubular cells. J Endocrinol 172:333–344. https://doi.org/10.1677/joe.0.1720333
32. Ghezzi C, Loo DDF, Wright EM (2018) Physiology of renal glucose handling via SGLT1, SGLT2 and GLUT2. Diabetologia 61:2087–2097. https://doi.org/10.1007/s00125-018-4656-5
33. Smith J, Tho LM, Xu N, Gillespie DA (2010) The ATM-Chk2 and ATR-Chk1 pathways in DNA damage signaling and cancer. Adv Cancer Res 108:73–112. https://doi.org/10.1016/B978-0-12-380888-2.00003-0
34. Brouwers B, Pruniau VP, Cauwelier EJ et al (2013) Phlorizin pretreatment reduces acute renal toxicity in a mouse model for diabetic nephropathy. J Biol Chem 288:27200–27207. https://doi.org/10.1074/jbc.M113.469486
35. Breyer MD, Qi Z, Tchekneva E (2006) Diabetic nephropathy: leveraging mouse genetics. Curr Opin Nephrol Hypertens 15:227–232. https://doi.org/10.1097/01.mnh.0000222687.75055.eb
36. Breyer MD, Tchekneva E, Qi Z et al (2007) Genetics of diabetic nephropathy: lessons from mice. Semin Nephrol 27:237–247. https://doi.org/10.1016/j.semnephrol.2007.01.001
37. Nchienzia H, Liao M-C, Zhao X-P et al (2019) Hedgehog interacting protein (Hhip) regulates insulin secretion in mice fed high fat diets. Sci Rep 9:11183. https://doi.org/10.1038/s41598-019-47633-3
38. Chang SY, Chen YW, Chenier I, Tran SM, Zhang SL (2011) Angiotensin II type II receptor deficiency accelerates the development of nephropathy in type I diabetes via oxidative stress and ACE2. Exp Diabetes Res 2011:521076. https://doi.org/10.1155/2011/521076
39. Liu F, Brezniceanu ML, Wei CC et al (2008) Overexpression of angiotensinogen increases tubular apoptosis in diabetes. J Am Soc Nephrol 19:269–280. https://doi.org/10.1681/ASN.2007010074
40. Brady JA, Hallow KM (2018) Model-based evaluation of proximal sodium reabsorption through SGLT2 in health and diabetes and the effect of inhibition with canagliflozin. J Clin Pharmacol 58:377–385. https://doi.org/10.1002/jcph.1030
41. Wanner C, Inzucchi SE, Lachin JM et al (2016) Empagliflozin and progression of kidney disease in type 2 diabetes. N Engl J Med 375:323–334. https://doi.org/10.1056/NEJMoa1515920
42. Neal B, Perkovic V, Matthews DR (2017) Canagliflozin and cardiovascular and renal events in type 2 diabetes. N Engl J Med 377:2099. https://doi.org/10.1056/NEJMc1712572
43. Perkovic V, Jardine MJ, Neal B et al (2019) Canagliflozin and renal outcomes in type 2 diabetes and nephropathy. N Engl J Med 380:2295–2306. https://doi.org/10.1056/NEJMoa1811744
44. Heerspink HJL, Stefánsson BV, Correa-Rotter R et al (2020) Dapagliflozin in patients with chronic kidney disease. N Engl J Med 383:1436–1446. https://doi.org/10.1056/NEJMoa2024816
45. Hinden L, Udi S, Drori A et al (2018) Modulation of Renal GLUT2 by the Cannabinoid-1 receptor: implications for the treatment of diabetic nephropathy. J Am Soc Nephrol 29:434–448. https://doi.org/10.1681/ASN.2017040371
46. Goestemeyer AK, Marks J, Srai SK, Debnam ES, Unwin RJ (2007) GLUT2 protein at the rat proximal tubule brush border membrane correlates with protein kinase C (PKC)-betal and plasma glucose concentration. Diabetologia 50:2209–2217. https://doi.org/10.1007/s00125-007-0778-x
47. Marks J, Carvou NJ, Debnam ES, Srai SK, Unwin RJ (2003) Diabetes increases facilitative glucose uptake and GLUT2 expression at the rat proximal tubule brush border membrane. J Physiol 553:137–145. https://doi.org/10.1113/jphysiol.2003.046268
48. Panchapakesan U, Pegg K, Gross S et al (2013) Effects of SGLT2 inhibition in human kidney proximal tubular cells–renoprotection in diabetic nephropathy? PloS one 8:e54442. https://doi.org/10.1371/journal.pone.0054442
49. Pirklbauer M, Schupart R, Fuchs L et al (2019) Unraveling reno-protective effects of SGLT2 inhibition in human proximal tubular cells. Am J Physiol Renal Physiol 316:F449–f462. https://doi.org/10.1152/ajprenal.00431.2018
50. Kim MN, Moon JH, Cho YM (2021) Sodium-glucose cotransporter-2 inhibition reduces cellular senescence in the diabetic kidney by promoting ketone body-induced NRF2 activation. Diabetes Obes Metab 23:2561–2571. https://doi.org/10.1111/dom.14503